ELSEVIER

Polymer 42 (2001) 3103–3113

polymer

www.elsevier.nl/locate/polymer

Morphological study of HDPE blown films by SAXS, SEM and TEM: a relationship between the melt elasticity parameter and lamellae orientation

A. Prasad[a,*], R. Shroff[a], S. Rane[b], G. Beaucage[b]

[a]*Equistar Chemicals, LP, 11530 Northlake Dr, Cincinnati, OH 45249, USA*
[b]*Materials Science and Engineering Department, University of Cincinnati, Cincinnati, OH 45221-0012, USA*

Received 8 October 1999; received in revised form 3 August 2000; accepted 4 August 2000

Abstract

Evidence is presented showing how the long relaxation times in the melt affect the subsequent morphology of blown films made from medium molecular weight (MMW) HDPE homopolymers. The blown film morphology was studied using the small-angle X-ray scattering (SAXS) technique, scanning electron microscopy (SEM) and transmission electron microscopy (TEM). SAXS data were used to obtain the lamellae orientation functions using the Herman's orientation function equation commonly used for wide-angle X-ray diffraction (WAXD). The blown film results showed an increase in orientation function with increase in E_R, a normalized melt elasticity parameter that reflects an increase in the longest melt relaxation times. In our study, such an increase in the longest relaxation times results from an increase in long-chain branching (LCB). As expected, compression molded samples show random orientation by SAXS. Considerable differences were observed in the lamella organization between the blown films of low and high E_R resins. TEM micrographs show the presence of fibril nuclei several microns long. Lamellae stack perpendicular to the machine direction (MD) in films made from higher E_R resins. In contrast, stacks of lamellae arranged randomly characterize the micrographs of blown films made from resins of low E_R value. A model is proposed to explain the relationship between orientation function and melt relaxation times.

Keywords: HDPE; Blown films; SAXS

1. Introduction

Polymeric films for packaging applications are commonly made from a variety of polyethylenes, e.g. low-density polyethylene (LDPE), linear-low-density polyethylene (LLDPE) and high-density polyethylene (HDPE), using a blown film process [1]. In such a process, a predominant deformation is applied in the machine direction (MD) while simultaneously being stretched in the transverse direction (TD). The polymer melt is shaped in the form of a bubble by blowing air from inside the bubble. An air ring is used around the bubble to cool the molten blown film and crystallization occurs in a short time (typically less than 2 s) under the influence of an elongational stress (and is concentrated at the frost-line height (FLH)).

The stress induced crystallization in blown films results in the formation of a row-nucleated crystalline structure as opposed to spherulite formation in the case of compression molded samples [2]. Keller [2] showed that in blown films the crystalline lamella overgrowth occurs epitaxially from the *c*-axis oriented fibril. As the lamellae grow outward, they gradually twist around the *b*-axis that stays perpendicular to the MD and the *a*- and *c*- axes are preferentially oriented along the MD with cylindrical symmetry about the *b*-axis. The preferential MD orientation of the *a*- and *c*- axes depends not only on the type of polyethylene but also on the processing or the fabrication conditions. At high orientation stress, there is a strong orientation of the *a*-axis parallel to the MD in LDPE [3], whereas in the case of HDPE the *c*-axis shows strong orientation parallel to the MD [4,5]. HDPE films can also display some *a*-axis orientation parallel to MD for low levels of stress.

A considerable amount of literature describes efforts made to understand the morphology of HDPE blown films and to relate the morphology with the solid state properties of the films [3–18]. The orientation of polymer chains and lamellar morphology are recognized as two important variables in determining the structure–property behavior of blown films [3,5,11,12,19–21]. The morphology of blown films generally depends on the overall processing parameters such as draw ratio, blow-up ratio, FLH, extruder temperature as well as on the molecular structural parameters such as molecular weight (MW), molecular weight

* Corresponding author. Tel.: +1-513-530-4368; fax: +1-513-530-4267.
E-mail address: a.prasad@equistarchem.com (A. Prasad).

0032-3861/01/$ - see front matter
PII: S0032-3861(00)00612-1

distribution (MWD) and long-chain branching (LCB). Considerable effort has been devoted to define the relationship between the processing conditions and the structure and properties of blown films [6,12,17,18].

It is a common practice in the literature to correlate chain orientation with solid state properties such as tear and tensile strength. Three common methods are used for the detection and characterization of chain orientation in polymers. They are FTIR dichroism, birefringence and wide-angle X-ray diffraction (WAXD); the latter is the most common method used for semicrystalline polymers [22,23]. The development of molecular orientation in the crystalline phase of the sample can be determined by measuring the alignment of its unit cell using the WAXD pole figure analysis. To describe the film anisotropy, one also needs quantitative information about the orientation of the molecules in the noncrystalline and interfacial phase regions.

PE films typically scatter strongly from [110] and [200] reflecting planes (corresponding to the *a*-axis and the *b*-axis) and a weak [002] reflection plane (*c*-axis) when the incident X-ray beam is normal to the film plane [24]. In order to evaluate the orientation of the crystalline phase, an intensity profile of a user selected annulus vs azimuthal angle is obtained from [110] and [200] reflections. The intensity for a given azimuthal angle will depend on the amount of appropriately oriented crystallographic planes that will allow diffraction at that angle.

For uniaxial orientation, the orientation distribution function of chain segments is defined by a series of orthogonal spherical harmonic orientation functions. Crystalline orientation will be characterized in terms of average squared cosine values that represent the average orientation of the normal to the crystalline plane with respect to each of the reference axes. The second harmonic orientation function is known as Herman's orientation function and is given by [25–27]:

$$f = \frac{3\langle \cos^2 \phi_{hkl,z} \rangle - 1}{2} \tag{1}$$

Where $\phi_{hkl,z}$ is the angle between the chain axis and a reference axis z, e.g. the MD.

$\langle \cos^2 \phi_{hkl,z} \rangle$ is defined as

$$\langle \cos^2 \phi_{hkl,z} \rangle = \frac{\int_0^{\pi/2} I(\phi) \cos^2 \phi \sin \phi \, \mathrm{d}\phi}{\int_0^{\pi/2} I(\phi) \sin \phi \, \mathrm{d}\phi} \tag{2}$$

where I is the intensity in photons and is defined as

$$I(\phi) = \int_0^{2\pi} \mathrm{I}(\phi, \beta) \, \mathrm{d}\beta \tag{3}$$

where $I(\phi,\beta)$ represents the intensity distribution measured on the pole figure of the (hkl) plane as a function of the angle α ($\pi/2 \geq \alpha \geq 0$) where $\alpha = \pi/2 - \phi$, and β ($2\pi \geq \beta \geq 0$).

When the chains are perfectly aligned along the reference axis, $f = +1$ ($\phi = 0°$), whereas $f = -1/2$ for chains aligned perfectly normal to the reference axis ($\phi = 90°$). For a perfect random orientation, $f = 0$. WAXD or FTIR dichroism techniques normally determine the function "f". Since [200] reflection contains information only about the *a*-axis, Eq. (1) is directly used to calculate f_a value. Without pure reflections from either the *b*- or the *c*-axis, one can use Wilchinsky's method [28] to obtain the information about *b*-axis and *c*-axis orientations. According to Wilchinsky, as long as one pure reflection is observed, one can combine the information obtained from the pure reflection (i.e. [200]) with the mix reflection (i.e. [110]) using Eqs. (4) and (5), to obtain f_b or f_c for a known crystal structure, e.g. orthorhombic.

$$\langle \cos^2 \theta \rangle_{110} = \mathrm{e}^2 \langle \cos^2 \phi \rangle + k^2 \langle \cos^2 \delta \rangle + g^2 \langle \cos^2 \epsilon \rangle \tag{4}$$

$$\langle \cos^2 \phi \rangle + \langle \cos^2 \delta \rangle + \langle \cos^2 \epsilon \rangle \tag{5}$$

where ϕ, δ, and ϵ are the angles between the *c*-, *b*- and *a*-axes and the reference axis, z, e.g. MD. Coefficients e, k and g are normally known for a given polymer crystal structure.

Lindenmeyer and Lusting [5] pointed out that merely qualitative knowledge of the *a*-axis and *b*-axis distribution may lead to erroneous conclusions concerning the *c*-axis distribution. To avoid this problem, they recommend measuring the *c*-axis distribution directly, using the very weak [022] reflection. In typical HDPE commercial blown films processes the polymer chains orient parallel to the MD (stress direction). Then, for such samples where a strong *c*-axis orientation function is expected, the pole figure analysis using the weak [022] reflection could give erroneous results.

The orientation of the noncrystalline phase can be obtained by the birefringence technique in combination with other techniques such as DSC and WAXD. Birefringence is a result of the polarizability of the anisotropic units that make up the polymer chain. Birefringence measures the total molecular orientation of a sample. However, knowledge of the intrinsic birefringence of the crystalline and amorphous regions of the polymer is essential to separate the crystalline orientation from the amorphous phase orientation.

Small-angle X-ray scattering (SAXS) is a well-known technique to characterize the nanometer scale microstructure of polymer [29,30]. SAXS is a study of X-ray scattering in reciprocal space at angles very close to the main beam, typically $2\theta < 2°$, where θ is half the scattering angle. SAXS depends on the occurrence of large-scale (10–500 Å) periodic heterogeneity in the structure and can provide a broad range of structural features [30,31]. SAXS measures the distance between lamella centers, which is in the range of hundreds of angstrom units. Most frequently, the only cooperative reflections that usually appear in the SAXS patterns occur because of the periodic arrangement of crystal lamellae along the chain-axis direction (stacked

lamellae). Therefore, SAXS is an ideal technique to investigate the orientation of lamellae with respect to the fabrication or stretching direction as opposed to chain orientation by the WAXD pole figure analysis (WAXD examines a size scale of 1–10 Å). In addition, SAXS can provide information on lamella thickness, provided the volume fraction crystallinity is known.

We have previously reported on the rheological and crystallization study of various grades of HDPE resins [32]. It was shown that the rheological characteristics and the quiescent isothermal crystallization rates were a strong function of the LCB content in HDPE resins, which were otherwise similar in melt index (MI), density, crystallinity, as well as MWD obtained from gel permeation chromatography (GPC) [32]. However, in that report [32] the effect of LCB on the blown film morphology was not studied. The purpose of the present work is twofold: to reveal the role of LCB in determining the lamellae orientation that develops in HDPE blown films by minimizing the MWD effect, and to examine the relationship between melt relaxation time and morphology in films prepared under similar extrusion conditions. In this respect, we have employed SAXS, scanning electron microscopy (SEM) and transmission electron microscopy (TEM) to explore local variations in the solid state structure of the films, in order to extend the current understanding of blown film morphology. No attempt was made to study the orientation of the unit cell because it has been studied previously by several authors using WAXD [6,12,17,18,22,23]. To our knowledge, SAXS has not been used to determine the orientation of lamellae in semicrystalline materials. Here we have made attempts to measure the lamellae orientation using Herman's orientation function (Eqs. (1) and (2)), which is normally applied to determining the crystallographic orientation function using WAXD.

2. Experimental

Commercial grade HDPE resins were employed in this study. Molecular, rheological, and thermal characteristics are listed in Table 1. These resins have similar MI, MWD and density, but different E_R (see discussion in Section 3.1). MI was measured as per ASTM D1238, condition F (190°C, 2.16 kg). The blown films were made under controlled conditions using a 4-in. monolayer Uni-flow die with a 44-mil die-gap and dual lip air ring. A 2.5-in. barrier polyethylene screw with a Maddox mixing section was utilized. The following conditions were used: melt temperature of 200°C, FLH of 11 in., blow-up ratio 2.5:1, output rate of 80 lb/h. The nominal film thickness was 1.5 mil (about 37.5 μm). The draw down ratio (DDR) was calculated to be 10.66 using Eq. (6):

$$\mathrm{DDR} = \text{Die gap}/(\mathrm{BUR} \times \text{Film gauge}) \quad (6)$$

The degrees of crystallinity of the pellets and film samples were determined from the heat of fusion using a Perkin-Elmer DSC 4 instrument at a heating rate of 5°C/min. The percent crystallinity was calculated by dividing the heat of fusion by 289 J/g [33]. The density, GPC and dynamic rheology experiments were carried out in the manner described previously [32].

Scattering data were obtained using a conventional pinhole SAXS camera and an X-ray diffractometer at Sandia and Oak Ridge National Laboratories. The lamellae orientation of the film was studied by SAXS. The 10-m 2-D pinhole camera was used to carry out SAXS experiments. A schematic of the experimental set-up is shown in Fig. 1a. The specimen to detector distance was 5 m and the angular divergence of the incident beam was less than 1 mrad. The reference direction was chosen to be the extrusion direction (MD). The *N* direction (ND) is normal to the film surface and TD is at right angles to both the MD and ND. While it would be desirable to obtain scattering patterns with beam incident along the MD and TD, this is difficult to do so due to the small thickness (<20 μm) available for scattering. Therefore, the scattering measurements on each material were made by stacking about 40 layers of films and directing the beam along the film thickness or ND direction (see Fig. 1b).

The SAXS scattering data are collected in the form of a 2-D image (see Fig. 2). A radial average is then performed on the 2-D scattering pattern, which is a quantitative measure of the intensity of X-ray scattering. From the radial average plots, the lamellae orientation function is determined using Herman's orientation function (see Eqs. (1) and (2)). The peak in the radial average curves is always very close to the MD. This direction was taken as the zero angle for calculation of Herman's orientation function in all cases. This

Table 1
Characteristics of HDPE resins

Sample	MI (g/10 min)	Pellet density (g/cm^3)	Film density (g/cm^3)	$M_w \times 10^{-5}$	M_w/M_n	E_R	$\eta_0 \times 10^{-4}$ (poise)[a]	T_m °C[b]	% X_c[b]
A	0.90	0.9617	0.9546	1.48	9.6	4.5	26.88	129.7	67.5
B	0.85	0.9604	0.9518	1.07	8.4	3.4	7.1	128.7	63.5
C	1.1	0.9623	0.9547	0.91	9.4	2.9	2.96	128.7	67.0
D	0.9	0.9595	0.9533	1.6	8.9	1.9	3.59	129.1	66.5

[a] Estimated zero-shear viscosity using the Sabia equation (see Ref. [28]) from the η^* vs ω plot at 190°C.
[b] First heat DSC experiments done at a heating rate of 10°C/min on "as is" blown film.

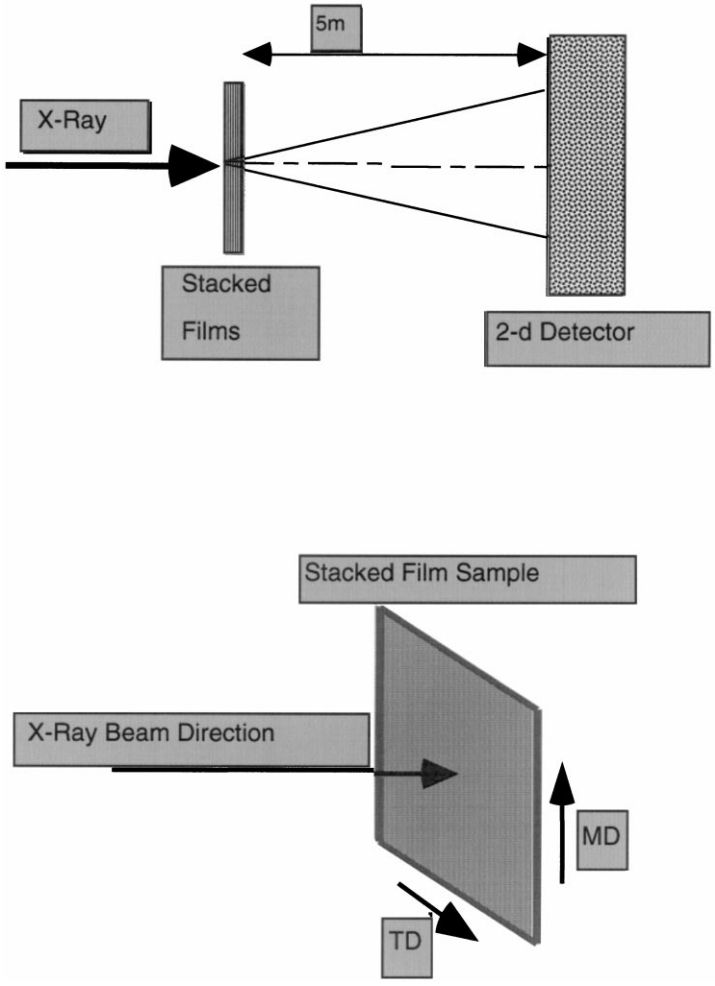

Fig. 1. Schematic of the experimental set-up of (a) the SAXS instrument and (b) blown film stacks with respect to the X-ray beam line.

orientation of the peak in scattering is consistent with the TEM and SEM images discussed below.

TEM experiments were performed according to the procedure of Yu and Wilkes [6]. The following sample preparation technique was used. A Reichert-Jung Ultracut-E ultramicrotome, with cryo-attachment, was used to prepare specimens of blown films for TEM analysis. The ultramicrotome cut 80-nm thick sections were stained in the manner described in Ref. [6]. The transmission electron microscope used for all imaging was a Joel TEM at 120 kV.

SEM experiments on blown films were performed using a Phillips XL 30 microscope operating at a voltage of 30 kV. The blown films were treated in heptane at 50°C for 30 min, washed in acetone and dried in a vacuum oven for 72 h at room temperature. Heptane etching makes lamellae more clearly visible in SEM micrographs. Samples were mounted on aluminum specimen mounts, coated on their bottom surface with a Ladd silver conducting paint and gold sputtered on their top to avoid sample charging.

3. Results and discussion

3.1. LCB and melt relaxation times

HDPE resins may contain low levels of LCB [32,34–37]. There are several factors that can lead to low levels of LCB: catalyst type, pelletization process, reactor hold-up time, etc. For typical HDPE samples, the level of LCB is so low as to be difficult to quantify by common techniques such as NMR, GPC and low-angle laser light scattering (LALLS) [37–39]. However, rheological data are very sensitive [32,35,38] to such low levels of LCB. It has been shown [32,35,36,39] that in commercial HDPE resins low levels of LCB can be related to a rheological parameter called E_R.

E_R is a melt elasticity parameter that reflects an increase in the longest melt relaxation times. E_R is independent of MW and temperature measurement, but is influenced by MWD and LCB. E_R utilizes linear viscoelastic data of the storage modulus, G', the loss modulus, G'', and the complex viscosity, η^*, in the frequency range 0.0158–400 rad/s. E_R is extracted from G' vs G'' data at

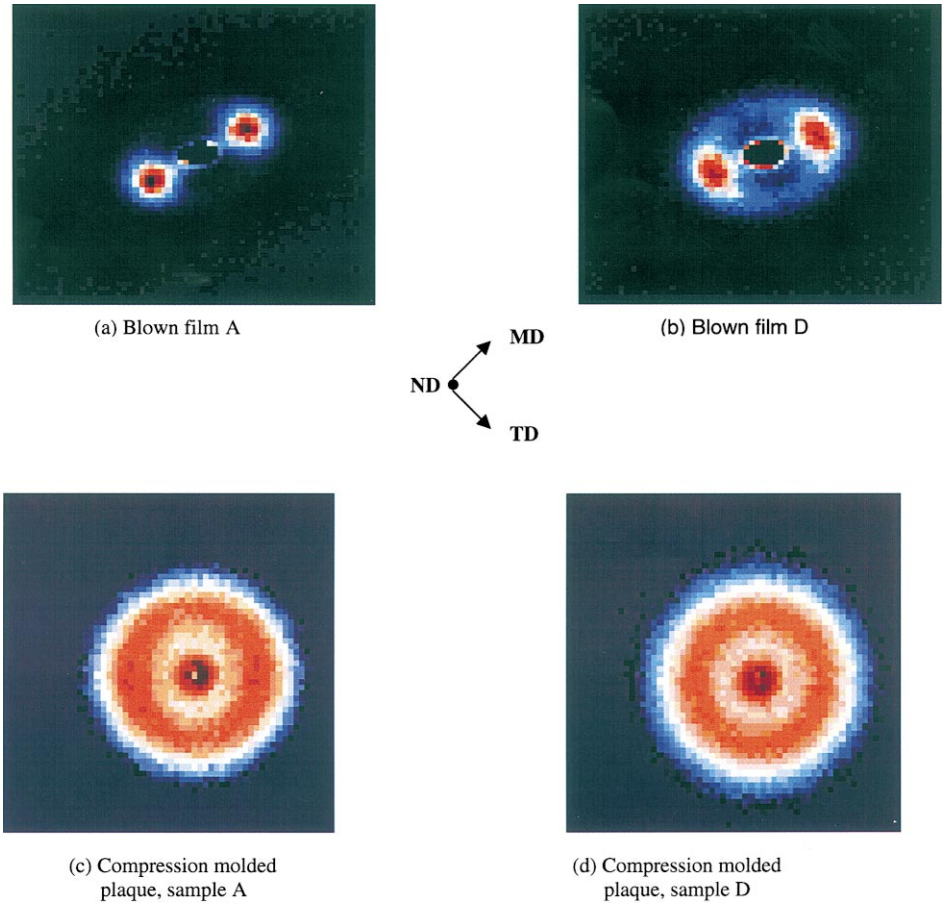

Fig. 2. A comparison of 2-D SAXS patterns of blown films with compression molded samples. For blown films the MD is consistently in the direction of the bright maximum.

the two lowest decades of frequency.

$$E_R = [C_1 G']_{\text{at } G''_{\text{ref}}} \tag{7}$$

where G''_{ref} is selected to be a low modulus value (corresponding to low frequencies) and C_1 is the normalization constant. For polyethylene melts, good results have been obtained with $G''_{\text{ref}} = 5000\ \text{dyn/cm}^2$ and $C_1 = 1.781 \times 10^{-3}\text{cm}^2/\text{dyne}$ [32,36]. When the available data do not extend down to G''_{ref}, extrapolation of data is made because the log–log plot of G' vs G'' is nearly linear in that region.

It was mentioned earlier that the measurement of E_R can be influenced by MWD and LCB. Fortunately the MWD effects can be separated from the LCB effects following the procedures of Shroff and Mavridis [36]. The resin in Table 1 with lowest E_R has lowest level of LCB [32]. We have shown [32] in HDPE resins that the LCB content strongly influences its quiescent crystallization rates. Therefore, it is relevant to understand at first the effect of LCB on the melt rheological properties of resins and how such molecular characteristics may affect the crystallization process and blown film morphology.

HDPE resins in Table 1 are characterized by a wide range of E_R or LCB. Thus, sample A has the highest level of LCB and sample D has the lowest LCB. First, the relationship between LCB and the melt relaxation times of HDPE resins are examined. Ramkummar et. al. [39]have described the method of determining the spectrum of relaxation times from the melt rheological data and we have followed their technique to obtain the relaxation spectrum in the melt. Therefore, here, only a brief discussion of the method is presented.

Computing the relaxation spectrum from experimentally measurable linear viscoelastic material properties has been the subject of numerous publications [39–43]. The experimental data used to determine the relaxation spectrum always include noise and are over a limited time or frequency range, both of which can affect the determination of the spectrum. Regularization with quadratic programming has been used to derive the spectrum [39–43]. The spectrum calculated from G'' alone is more accurate at shorter relaxation times, while that from G' data alone is more accurate at longer relaxation times. Ramakummar et al. [39]have shown that the most accurate relaxation spectrum is obtained by scaling the spectrum using the regularization scheme of Honerkamp et al. [42], by extending the spectrum about two logrithmic decades on either side of the

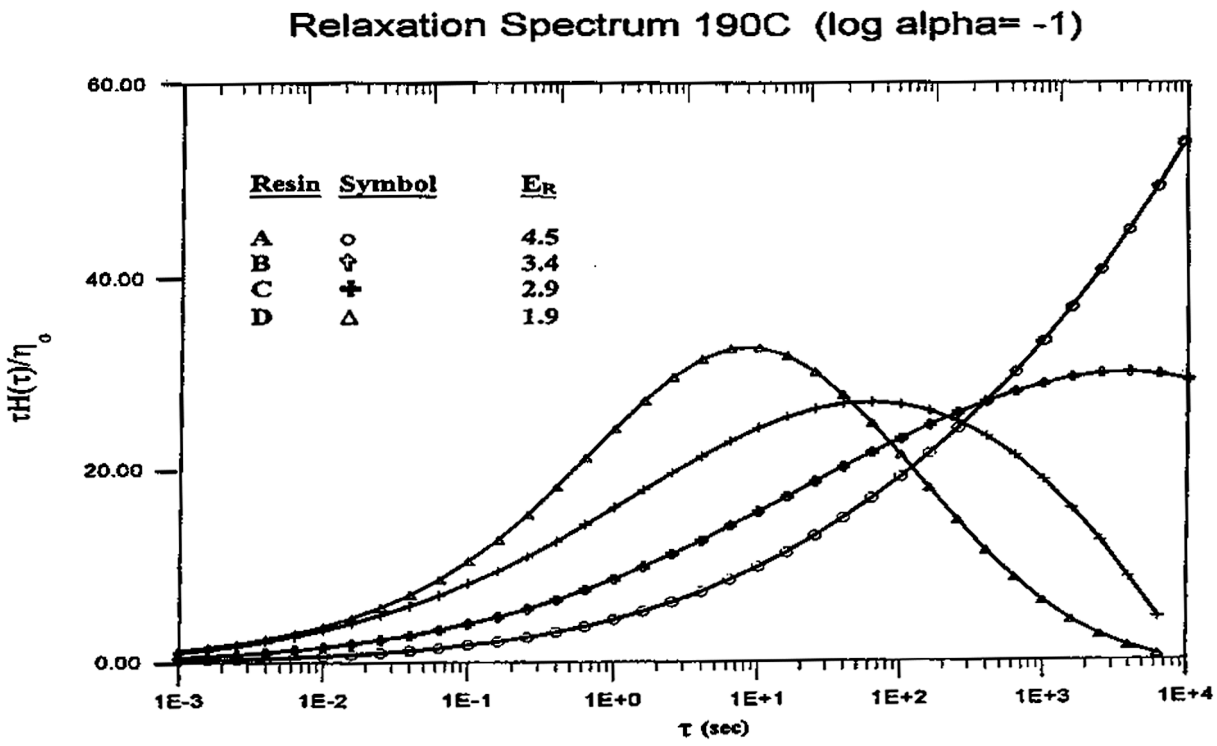

Fig. 3. Normalized relaxation spectrum of the four commercial HDPE samples obtained using the linear viscoelastic data as a function of E_R. (O) sample A, (⇧) sample B, (+) sample C and (△) sample D.

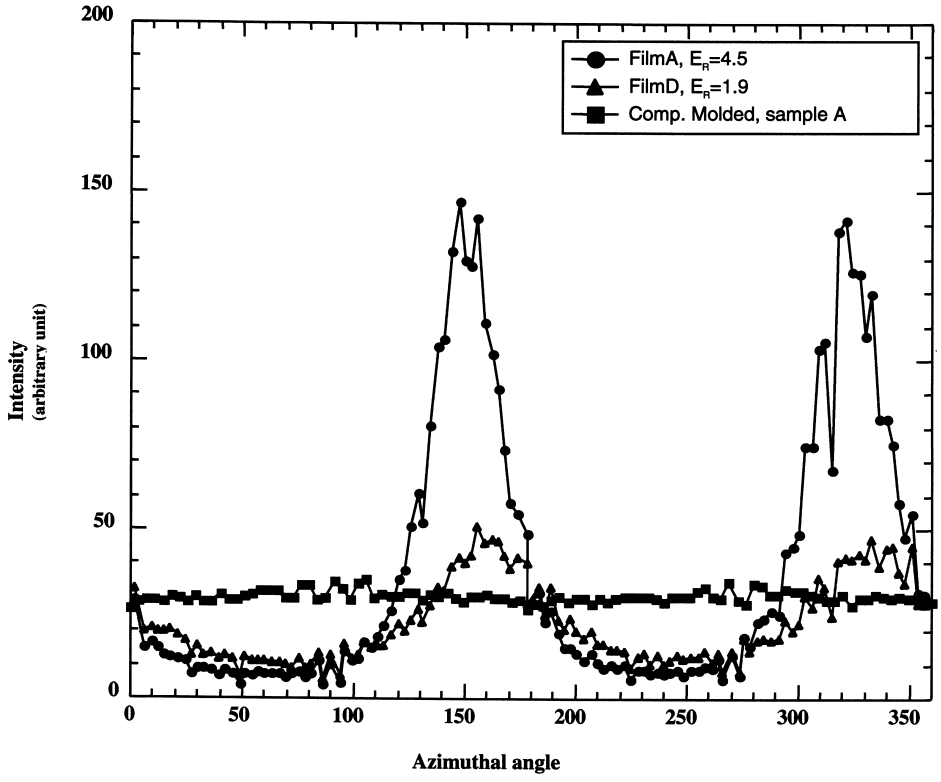

Fig. 4. Intensity against azimuthal angle plot of 2-D SAXS patterns in Fig. 2. The sample designation is shown in the inset. For the blown films the MD is consistently in the direction of the peak, the zero angle for calculation of the orientation function is taken at the maximum of the first peak consistently since this is the machine direction.

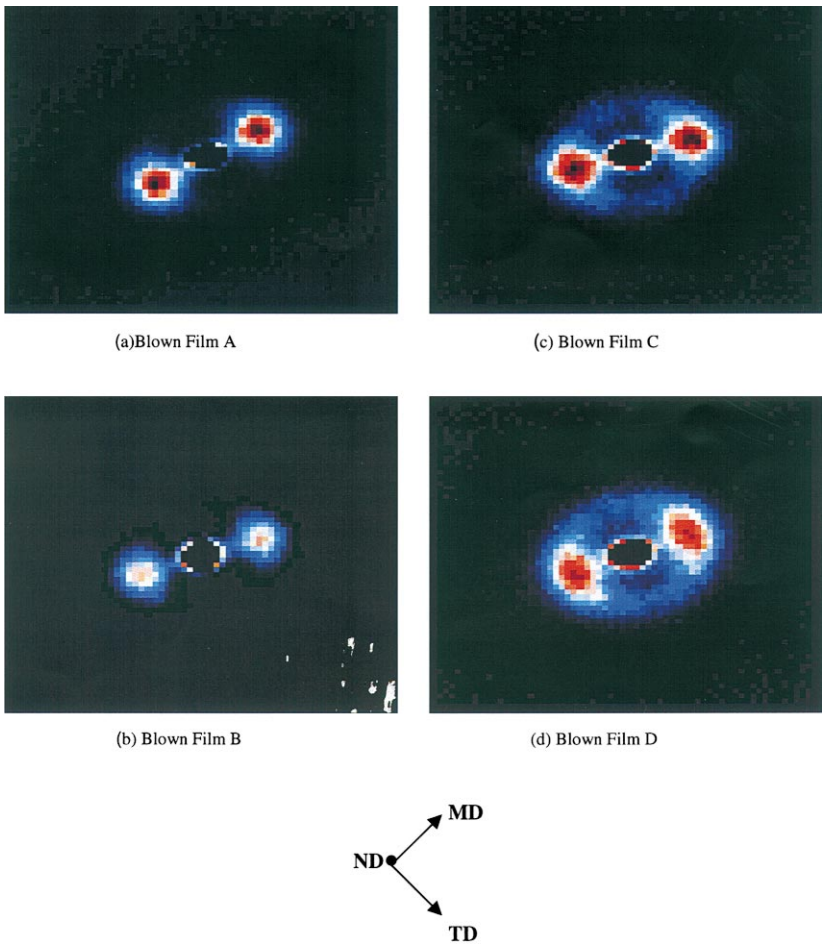

Fig. 5. A comparison of 2-D SAXS patterns of HDPE blown films as a function of LCB. The MD is in the direction of the bright maxima in all cases.

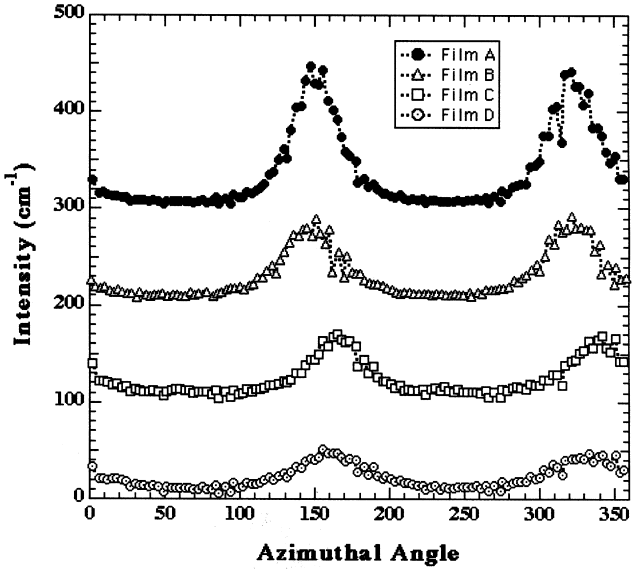

Fig. 6. Intensity against azimuthal angle plot of 2-D SAXS pattern in Fig. 5. The sample designation is the same as in Fig. 5. For the blown films the MD is consistently in the direction of the peak, thus the zero angle for calculation of the orientation function is taken at the maximum of the first peak.

frequency range of the input data, and by using a blended function of G' and G'' data to minimize the error in regenerating the original experimental data.

The relaxation spectrum is derived from the linear viscoelastic data on the polymer melts at 190°C. The relationship between the measured dynamic storage modulus, G', loss modulus, G'', and the relaxation spectra is given by the following equations [44]:

$$G'(\omega) = \int_{-\infty}^{+\infty} H(\lambda) \frac{(\omega\lambda)^2}{1 + (\omega\lambda)^2} \, \mathrm{d}\log\lambda \tag{8}$$

$$G''(\omega) = \int_{-\infty}^{+\infty} H(\lambda) \frac{(\omega\lambda)}{1 + (\omega\lambda)^2} \, \mathrm{d}\log\lambda \tag{9}$$

where $H(\lambda)$ represents discrete relaxation modes, λ represents discrete relaxation times, and ω is the frequency. The relaxation spectra can be calculated from the G' and G'' expression and is normalized by dividing by zero-shear rate viscosity (η_0).

In Fig. 3, the normalized relaxation spectrum of the four HDPE resins are shown where we have plotted $\tau H(\tau)/\eta_0$ as a function of relaxation time τ. It can be seen that the long

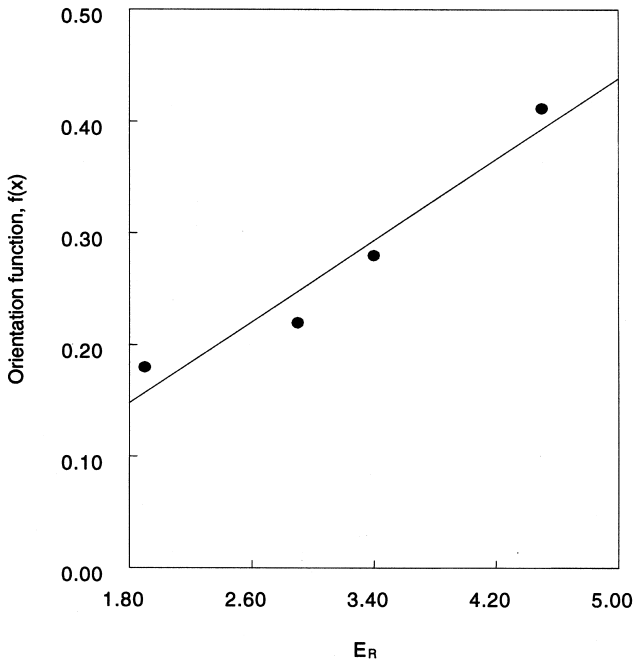

Fig. 7. Plots of lamellae orientation function $f(x)$ against melt elasticity parameter E_R. The solid circles represent HDPE film data and the solid curve represents the best fit through the data points.

relaxation times are strongly influenced by the amount of LCB. For example, lower E_R materials show peak relaxation times of the order of 10–100 s. The peak relaxation time shifts to a higher value with the increase in E_R. For example, the peak in the relaxation spectrum of sample A ($E_R = 4.5$) is not even observable within the accessible experimental data range, indicating extremely long relaxation times in the melt. The significance of the melt relaxation times and lamellae orientation will be discussed later.

3.2. 2-D SAXS patterns

The 2-D SAXS patterns from melt-crystallized isotropic samples typically display a strong first-order diffraction ring and one or two higher orders of much lower intensity. The SAXS pattern of an oriented sample typically displays strong two-point patterns with a maximum in the draw direction or at a certain angle about the reference direction. Fig. 2 shows a comparison of 2-D SAXS patterns of blown films and compression molded plaques. In this example we have compared sample A and D blown films with their respective compression molded plaques. The dark spot in the center of the scattering pattern is due to the main X-ray beam stop. Caution should be exercised here in comparing the 2-D SAXS patterns. The 2-D plots can only give an indication of whether the lamella is oriented (two or more bright maxima) or whether it is isotropic (complete ring). One cannot estimate the degree of orientation in the case of samples that are oriented to a similar degree, by just looking at the 2-D plots. For quantitative comparison intensity vs azimuthal angle plots such as the one shown in Fig. 4 should be used.

The 2-D SAXS patterns of compression molded samples are characterized by two diffuse halo rings indicating isotropicity in the sample (Fig. 2c and d). The scattering patterns of blown films are quite different. An intense and sharp two-point with negligible scattering on the equator is seen in Fig. 2a and b. The scattering intensity of the two lobes seems to decrease with E_R. A radial average was performed on all the 2-D scattering patterns to calculate the scattering intensity as a function of the azimuthal angle, Ψ. A plot of scattering intensity vs Ψ is shown in Fig. 4. It is clearly seen that samples A and D have two distinct scattering maxima at about 160 and 340° angles with respect to the X-ray beam direction. The angle axis in the azimuthal plot, Fig. 4, is relative to the SAXS image. The peak in the SAXS patterns consistently points in the MD relative to the sample indicating that the lamellae are normal to the MD. Samples were run at a tilt angle to take advantage of the corners of the square image. However, the peak intensity values of the two resins are quite different. Sample D has a lower intensity value when compared with sample A. This means that the lamellae in the sample A film are highly orientated with respect to the MD as compared with the more random orientation of the lamellae in the sample D film. The compression molded plaques show a completely different behavior. As expected, compression molded plaques do not show a maximum in the intensity vs. azimuthal angle plot due to isotropicity in lamellae orientations.

Composite plots of 2-D SAXS patterns and radial average plots are shown in Figs. 5 and 6, respectively, for all the HDPE films studied. The 2-D SAXS patterns for all the samples show two sharp intense spots at certain scattering angles. However, significant differences in the scattering intensity can be seen as a function of E_R. For example, sample A ($E_R = 4.5$) shows a strong preference for orientation of the lamellae's normal parallel to the MD direction as characterized by two intense scattering spots in Fig. 5a. As the E_R value decreases, the intensity of the two sharp spots diminishes but still shows preferred orientation in the MD direction. This can also be seen in the plot of Fig. 6, where it is clearly shown that the scattering intensity diminishes for lower E_R materials. As E_R increases, the population of lamella normal parallel to the MD increases, as evidenced by an increase in the scattering intensity of Fig. 6. The peaks are consistently in the MD direction.

Eqs. (1) and (2) (Herman's orientation function) were used to calculate the orientation functions of the lamellae. The data of Fig. 6 were used in Eq. (2) to solve for $\cos^2 \Psi$ by the numerical integration process. Then the $\cos^2 \Psi$ values were used in Eq. (1) to calculate numerically the lamellae orientation function values, $f(x)$, the zero position for Ψ is taken at the leftmost peak that points consistently in the MD direction for these samples. Fig. 7 shows a plot of E_R against orientation function. The filled circles represent data points obtained on HDPE blown films in Table 1. It is important to

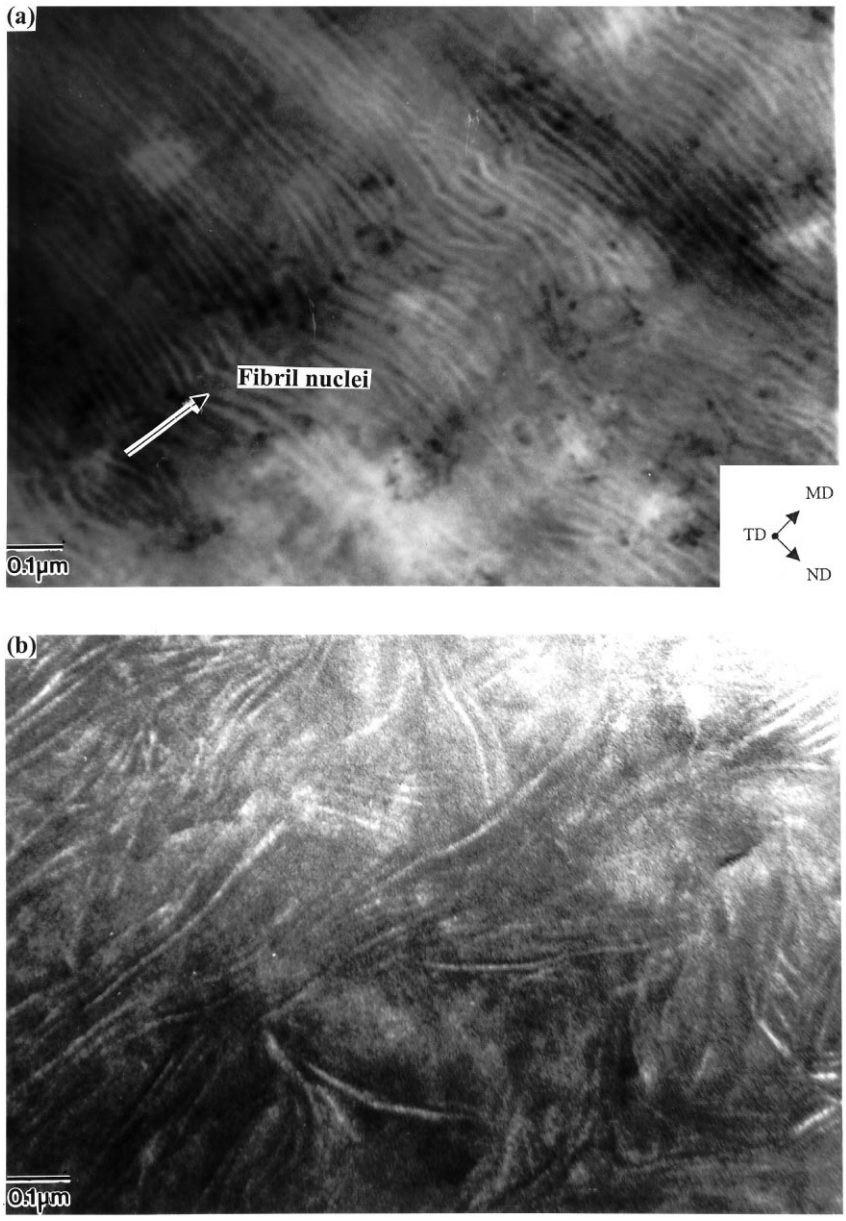

Fig. 8. TEM micrographs of blown films: (a) higher E_R sample A and (b) lower E_R sample D.

realize that the data in Fig. 7 can not be extrapolated linearly because resins with lower than 1.9 E_R value are not available. The plot of Fig. 7 indicates that the lamellae orientation is strongly influenced by the amount of LCB and increases with E_R. Thus, under similar extrusion conditions, the film made with a higher E_R material has a distinctly higher value of the orientation function.

In a recent paper, Yu and Wilkes have shown by IR dichroism that the amorphous phase orientation is very small in an HDPE blown film [45]. Thus, besides the orientation of amorphous regions, which in our study is assumed to be small and similar for the blown films, the arrangement of lamella structure has the dominating influence on the film morphology. From the orientation study it is obvious that lower E_R materials promote random orientation of lamellae in blown films.

3.3. TEM and SEM results

The TEM micrographs of the blown films made from resin A ($E_R = 4.5$) and resin D ($E_R = 1.9$) are shown in Fig. 8a and b. The MD, TD and ND are shown on the micrographs. Considerable differences are seen in the lamella organization between the two samples. In film D, the lamellae do not exhibit preferential orientation of their lateral dimensions and are randomly oriented with respect to the MD. The lamellae have a thickness of 8–13 nm. On the other hand, in Fig. 8a, well-oriented and well-defined stacked

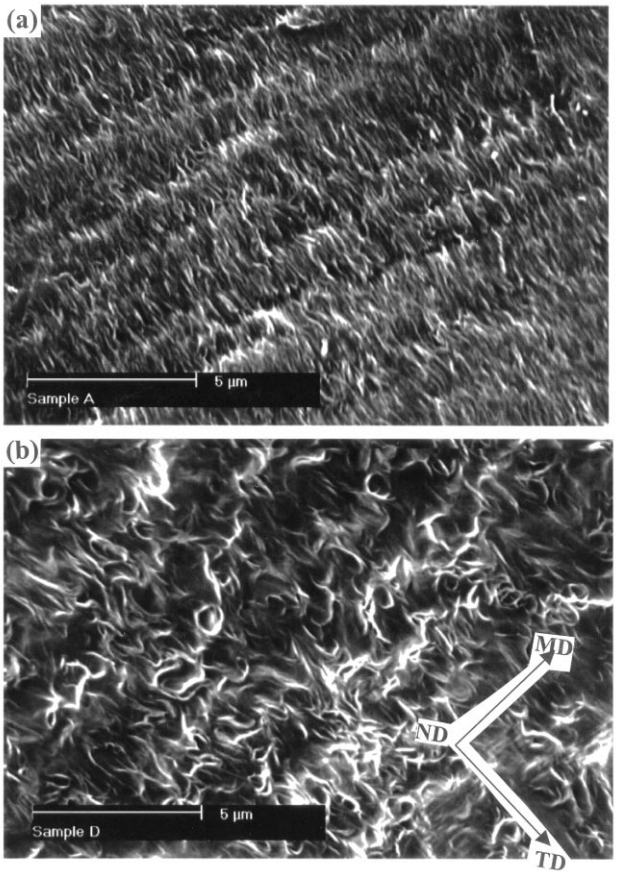

Fig. 9. SEM micrographs of blown films: (a) higher E_R sample A and (b) lower E_R sample D.

lamellae and distinguishable amounts of row-nucleated fibril structures in the MD direction are distinctly visible. One set of fibril nuclei is shown with an arrow in Fig. 8a. Film A shows considerable stacking of the lamellae long dimensions perpendicular to the MD and has a similar lamella thickness to film D. The morphology of film sample B (not shown here) is similar to sample A, but fibril nuclei were not readily seen in the TEM micrographs of sample B. The TEM micrographs further support the SAXS findings described above.

Similarly, SEM micrographs for the two blown films of samples A and D are shown in Fig. 9a and b. Once again, the two micrographs show different organization of stacks of lamellae. Sample A (high E_R) shows stacks of lamellae oriented in the MD direction. In the film of sample D, the lamellae stacks are randomly oriented. Thus, SAXS, TEM and SEM have shown results that are qualitatively similar. However, one cannot obtain quantitative information for the extent of lamellae orientation from the TEM and SEM micrographs.

Yu and Wilkes [45] have reported similar types of morphology in uniaxially oriented tubular films of HDPE as a function or MWD. They showed that the broader MWD resin formed fibril nuclei (row structure) in blown films that were not evident in the narrower MWD resin. The results of Yu and Wilkes may not be easily applied to this study because of two reasons. First, we have minimized the variation in MWD of the resins and any observed rheological differences are ascribed to small levels of LCB in essentially linear PE. Second, our blown films have some biaxial orientation due to blow-up ratios greater than unity. We have observed the appearance of fibril nuclei only in blown films of HDPE resins that contain higher levels of LCB. Thus it seems that broader MWD, as well as higher levels of LCB of similar MWD resins have a tendency to form fibril nuclei and stacking of lamellae in the MD direction in blown films.

3.4. Orientation and E_R

The reason for the strong dependence of orientation function on E_R (amount of LCB) in Fig. 7 can be attributed to the differences in the melt relaxation times of the resin. In the extruder and die, polymer melts experience high shear rates ($>100\ s^{-1}$), which causes the polymer melt to experience some degree of molecular orientation. After the die exit and before the FLH, polymer melts relax and at the same time also experience a high tensile force or stress in the machine direction. The extent to which molecular relaxation can occur and tensile stress develops is dictated by the melt relaxation times. The longest molecules and molecules with long chain branching are more likely to form entanglements that act as temporary cross-links, leaving the faster relaxing short molecules relatively free to disorient. The higher oriented melt results in fibril nuclei and promotes formation of highly row-nucleated, uniaxial lamellae stacking in the MD [6]. Furthermore, we have shown that higher E_R resins promote faster crystallization rates under a quiescent condition [32]. Under strain conditions, it is expected that higher E_R resins will crystallize even faster. Consequently, this would further impede the relaxation process of higher E_R resins while crystallizing. As a result SAXS shows high lamellae orientation functions for the higher E_R materials in the MD. In the case of lower E_R materials where the zero-shear viscosity is lower and relaxation times are shorter, it is expected that random orientation of the lamellae will result due to fewer fibril nuclei formations.

4. Conclusions

SAXS is a useful technique for measuring the lamellae orientation in blown films. Compression molded plaques of low and high E_R resins show random orientation of lamellae by SAXS. Blown films show vastly different results. Blown films of lower E_R resins show random orientation of lamellae, whereas high E_R resins show a greater degree of lamellae stacking in the MD direction (high orientation function value). TEM and SEM micrographs support the SAXS observation. The orientation function measured by SAXS increases with E_R. Under similar process conditions, blown

films of higher E_R resins have a higher value of orientation function.

Acknowledgements

Authors acknowledge the help of Ms Sharon Chang, Tina Kalemanis and Amy Weiskittel for the TEM and SEM experiments. The SAXS patterns were taken on the 10-m SAXS camera at Oak Ridge National laboratory with the assistance of Dr J.S. Lin.

References

[1] White JL, Cakmak M. In: Mark HF, Kikales N, Overberger C, Menges G, editors. Encyclopedia of polymer science and engineering, 10. New York: Wiley-Interscience, 1987. p. 619.
[2] Keller A, Machin MJ. Macromol Sci (Phys) B 1967;1:41.
[3] Desper CR. J Appl Polym Sci 1969;13:169.
[4] Rogers CE, Semanik JR, Kapuer S. Structure and properties of polymeric films. New York: Plenum Press, 1973.
[5] Lindenmeyer PH, Lusting S. J Appl Polym Sci 1965;9:227.
[6] Ta-Hua Yu, Wilkes GL. Polymer 1996;37:21.
[7] Pearson JR, Petrie CJ. J Fluid Mech 1970;40:1.
[8] Han CD, Park YJ. J Appl Polym Sci 1975;19:3257.
[9] Choi K, White JL, Spruiell JE. J Appl Polym Sci 1980;25:2777.
[10] Kanai T, White JL. Polym Engng Sci 1984;24:1185.
[11] Maddams WF, Preedy JE. J Appl Polym Sci 1978;22:2721.
[12] Gupta A, Simpson DM, Harrison IR. J Appl Polym Sci 1993;50:2085.
[13] Holmes DR, Palmer RP. J Polym Sci 1958;31:345.
[14] Haber A, Kamal M. Plast Engng 1987;10:43.
[15] Fruitwala H, Shirodhkar P, Nelson PJ, Schregenberger SD. J Plast Film Sheet 1995;11:298.
[16] Kanai T, Kimura M, Asano Y. J Plast Film Sheet 1986;2:224.
[17] Shukhadia A. J. Plast Film Sheet 1994;10:213.
[18] Shukhadia A. SPE ANTEC Proc 1998;44:160.
[19] Tagawa T, Ogura K. J Polym Sci, Polym Phys Ed 1980;18:971.
[20] Sherman ES. Polym Engng Sci 1984;24:895.
[21] Dormier EJ, Brady JM, Chang WH, Schregenberger SD, Barnes JD. SPE ANTEC Proc 1989;35:696.
[22] Wilkes GL. Adv Polym Sci 1971;8:91.
[23] Ward IM. Adv Polym Sci 1985;66:81.
[24] Alexander LE. X-ray diffraction methods in polymers science. New York: Wiley, 1969.
[25] Samuels RJ. Structured polymer properties. New York: Wiley, 1974.
[26] Wilkes GL. In: Mark HF, Kikales N, Overberger C, Menges G, editors. Encyclopedia of polymer science and engineering, 14. New York: Wiley-Interscience, 1988. p. 542.
[27] White JL. In: Mark HF, Kikales N, Overberger C, Menges G, editors. Encyclopedia of polymer science and engineering, 10. 1988. p. 595.
[28] Wilchinsky ZW. J Appl Phys 1960;31:1969.
[29] Kakudo M, Kasai N. X-ray diffraction by polymers. New York: Elsevier, 1992.
[30] Debye PH, Anderson R, Brumberger H. J Appl Phys 1957;28:679.
[31] Guinier A, Fournet G. Small-angle scattering of X-rays. London: Wiley, 1955.
[32] Shroff R, Prasad A, Lee C. J Polym Sci, Polym Phys Ed 1996;34:2317.
[33] Alamo RG, Mandelkern L. Macromolecules 1989;22:1273.
[34] Hogan JP, Levett CT, Werkman RT. SPE J 1967;23:87.
[35] Shroff RN, Mavridis H. J Appl Polym Sci 1993;49:299.
[36] Shroff RN, Mavridis H. Macromolecules 1999;32:8454.
[37] Hughes JK. SPE ANTEC Proc 1983;29:306.
[38] Dickie BD, Koopmans RJ. J Polym Sci C 1990;28:193.
[39] Ramkummar D, Caruthers J, Mavridis H, Shroff RN. J Appl Polym Sci 1997;64:2177.
[40] Laun HM. J Rheol 1986;30:459.
[41] Baumgaertel M, Winter HH. Rheol Acta 1989;28:511.
[42] Honerkamp J, Weese J. Macromolecules 1989;22:4372.
[43] Orbey N, Dealy JM. J Rheol 1991;35:1035.
[44] Graessley WW. Adv Polym Sci 1974;16:1.
[45] Ta-Hua Yu, Wilkes GL. J Plast Film Sheeting 1997;13:299.